

Neutron scattering in ^{189}Os for nucleosynthesis rates of the odd- A Os isotopes and nucleochronology

M. T. McEllistrem, R. R. Winters,* R. L. Hershberger,[†] Z. Cao,[‡]
R. L. Macklin,[§] and N. W. Hill[§]

Department of Physics and Astronomy, University of Kentucky, Lexington, Kentucky 40506

(Received 6 September 1988)

Neutron elastic and inelastic scattering cross sections have been determined for neutrons incident on ^{189}Os at three very low energies. Cross sections for scattering to the ground state and 36.2-keV excited level have been measured for incident energies of 63.5 and 73.3 keV, and also to the 69.6-keV excited level at 97.5-keV incident energy. These measurements are combined with neutron scattering cross sections for ^{187}Os , neutron capture cross sections, and other low-energy scattering observables to provide a basis for a single, consistent model of all data for both odd- A Os isotopes. The properly interpreted capture rates are important for the Re/Os nucleochronology and for s -process nucleosynthesis rates. The elastic and inelastic scattering cross sections provide a very-low-energy test of statistical model-flux distributions; model accuracy at very low energies is an important issue for reaction rates used in nucleosynthesis estimates.

I. INTRODUCTION

The galactic and terrestrial abundances of the Os isotopes reflect formation in massive stars through s -process capture, and also formation through β decay back toward the nuclear stability valley from highly neutron rich nuclei formed in rapid, sequential neutron capture (r process). Clayton¹ had shown that ^{186}Os was effectively shielded from the r -process β -decay chain because ^{186}W is stable, terminating the chain before Os. Thus, ^{186}Os is formed and destroyed through the neutron capture rates of the s process only. Part of the ^{187}Os abundance is also formed through s -process capture; that part is then in the stochastic equilibrium defined by relative neutron capture cross sections. The rest of the ^{187}Os abundance is formed indirectly from the sequential β decay of highly neutron rich nuclei formed in the r process. The ^{187}Os is destroyed, though, only in the s process, by capture to ^{188}Os . If the s -process relative abundances of these Os isotopes can be accurately calculated, the excess abundance of ^{187}Os would be attributable to β decay from ^{187}Re , and can be used to test nucleosynthesis duration.¹

To test nucleosynthesis rate estimates, the decay half-life of ^{187}Re must be known. The terrestrial half-life of ^{187}Re has been determined using geochemical methods² to be 45.5 Gyr. Recent and more accurate mass spectrometric methods³ now yield a half-life of 42.3 ± 1.3 Gyr, a very appropriate half-life to date periods measured in tens of Gyrs. There is still a problem of knowing the effective half-life for nucleosynthesis, since the ^{187}Re decay rate in the interior of stars may be different than that measured on earth.⁴ The effective half-life needed to date nucleosynthesis reflects the uncertain residence time of Re in stars. This uncertainty could lead to as much as a 20% uncertainty in the duration of nucleosynthesis.⁴

The need to determine the s -process abundance of ^{187}Os led to careful measurements and remeasurements of

the appropriate capture cross sections in two laboratories.^{5,6} The results are confidently known ground-state capture rates, from which s -process abundances were determined, and nucleosynthesis duration, or galactic age determinations, were made.⁶

A modification of measured capture rates is necessary for the stellar environment, though, because the temperature is high enough in massive stars that the first excited level of ^{187}Os is more strongly illuminated by neutrons than the ground state; the excited level capture rate can only be calculated.⁷ Reliable calculation of capture from the excited level requires accurate knowledge of the neutron reaction rates for nuclei in this mass region. For this reason two earlier neutron scattering experiments were completed, one addressing inelastic scattering cross sections for 34 keV neutrons,⁸ and the other both elastic and inelastic scattering cross sections for 60 keV neutrons⁹ incident on ^{187}Os . Measured total cross sections,¹⁰ and other neutron scattering observables¹¹ referred to 1 eV were combined into both phase shift and complex potential analyses which fit well all of the data.⁹ Accurate knowledge of the models which properly describe neutron total cross sections, elastic and inelastic scattering cross sections as well as ground-state neutron capture cross sections, means that excited level capture rates can be confidently calculated.

Doubt about the accuracy of knowledge of the excited-state capture rate persists, however, for at least two reasons. One is that the statistical model, or compound nucleus model, projects average neutron capture strengths which depend on the angular momentum (J) of the capturing state. Other capture mechanisms could lead to capture strengths independent of J , which would alter⁷ the ratio of excited level to ground-state capture in ^{187}Os . It is this ratio which is important for estimating the s -process destruction of ^{187}Os . The assumption of J -dependent vs J -independent γ -ray strength affects the

capture ratio because the $\frac{3}{2}^-$ excited level leads to higher J states in capture than does the $\frac{1}{2}^-$ ground state.

A second source of doubts could arise because the scattering model analysis of the previous study⁹ included several different forms of statistical models, with little differentiation amongst them. Since that time it has become clear that the model as developed by Tepel, Hofmann, and Weidenmuller,¹² which accounts for both level-width fluctuations and channel-channel correlations, provides an accurate representation of nucleon induced reactions for incident energies where the compound system reaction mechanisms are dominant.¹³⁻¹⁵ The more recent approximation of the model of Tepel, Hofmann, and Herman¹⁶ provides an even more accurate account of statistical-model cross sections. Both of these forms provide the same results for low-energy neutron scattering,^{14,17} and also the same results as the most recent form of the model as developed by Moldauer.¹⁸

A direct test of the potential and statistical models is made possible by combining the present study of neutron interactions with ¹⁸⁹Os with previously published results^{5,9,19} for ¹⁸⁷Os. The nuclear structures of these two odd- A Os isotopes are essentially the same, with the same active nucleon configurations, and the same deformation,²⁰ except that the $\frac{1}{2}^-$ and $\frac{3}{2}^-$ levels are reversed in energy order, with the $\frac{3}{2}^-$ level being the ground state in ¹⁸⁹Os. Thus, if scattering, total, and neutron capture cross sections could be measured for this nucleus, and if these new data could be combined successfully into a model which describes scattering and capture from both Os nuclei, then that would be a highly credible basis for projecting the neutron capture rate ratios for both the $\frac{1}{2}^-$ and $\frac{3}{2}^-$ levels, and therefore the capture rates appropriate for both levels of ¹⁸⁷Os in stars.

More information than suggested above is available from the present ¹⁸⁹Os study. Although the two levels indicated account for all but a very small fraction of the stellar capture, the rest comes from capture on a $\frac{5}{2}^-$ level at about 74 keV excitation energy in ¹⁸⁷Os. Scattering studies near an incident neutron energy of 100 keV would show scattering cross sections to the corresponding $\frac{5}{2}^-$ level at 69.6 keV in ¹⁸⁹Os. Thus, the small role of that level in stellar capture can also be included with considerable confidence.

The results of this study are that a single model accounts quite well for scattering and neutron capture cross section ratios in both Os nuclei, and the corrected statistical model¹⁶ distributes well the absorbed neutron flux into the different open scattering channels. We are able to show also that the effects of neutron capture from the excited levels of ¹⁸⁷Os are quite independent of stellar temperature in the range from 10 to 100 keV, lending further credence to the suggestion that this correction to galactic age determination, or stellar Os nucleosynthesis, is well determined.

II. EXPERIMENTAL METHODS AND PROCEDURES

The experimental system used for these measurements was the same as that used for the earlier experiment⁹ except for the form, size, and shape of the scattering sam-

ples. Incident neutrons were obtained from the ⁷Li(p,n) reaction using protons from the University of Kentucky 6.5-MV accelerator incident on thin LiF targets evaporated onto Ni backings. The circular Ni disc terminated the beam line, and was air cooled. The incident proton energy was determined by measuring the ⁷Li(p,n) threshold with a long counter,²¹ and then setting the energy with respect to the threshold. The threshold was remeasured several times during the course of the experiment, and found to be stable to within ± 0.1 keV. The ⁷Li(p,n) yield curves above threshold also served to measure the LiF target thickness, which was maintained at about 2 keV.

The accelerator was operated in pulsed-beam mode with beam pulses of < 3 ns width at a repetition rate of 5 MHz. Neutron velocity spectra were measured in time-of-flight (TOF) mode with two NE110 scintillation detectors. Both scintillators were rectangular, 5.7×5.7 cm, and about 1.9-cm thick. Both were surrounded by graded shields of thin layers of Al, Fe, Cu, and Pb to absorb low-energy electromagnetic radiation reaching the detectors. One scintillator was optically coupled to two photomultipliers operated in coincidence, and mounted at 0° to measure incident neutron energy and energy spread. The detector was located at 3.615 m from the LiF target, and energies were determined by timing neutron TOF peaks with respect to the prompt γ peak from the target. This detector indicated a 0° energy spread of about 6 keV, roughly consistent with the LiF target thicknesses. The evaporated LiF targets ranged in thickness from 1.7 to 2.0 keV for 1.9 MeV protons; reaction kinematics then leads to neutron energy spreads from about 4.2 to 5.5 keV.

The second scintillation detector was the majority logic detector²² obtained from the Oak Ridge Electron Linear Accelerator (ORELA) laboratory at Oak Ridge National Laboratory (ORNL) for this experiment. That detector was mounted at 90° to detect sample scattered neutrons, and housed in a heavy paraffin and Pb shield.⁹ The 90° detector was also shadowed from the LiF target by blocks of W and Cu. These extensive shielding measures were necessary to reduce the background to the point that sample spectra with good statistics could be obtained for the small inelastic scattering peaks.

Two scattering samples were used. One was the ¹⁸⁹Os sample, which was eight thin circular disks, each 1.27 cm in diameter. They were packaged together to make a cylindrical scattering sample 0.46-cm high by 1.27-cm diam. An identical size Pb sample was fabricated to provide a scattering sample with no inelastic scattering, so that the detector response for a single, isolated peak could be well determined in the identical scattering geometry as that of the Os sample. The Os was enriched in ¹⁸⁹Os to 94.5%, with 3.28% of ¹⁹⁰Os and 1.33% of ¹⁹²Os as the most abundant contaminants. Since neither of these isotopes has inelastic scattering below 190 keV, they posed no problem for measurements of inelastic scattering yields. The inelastic scattering yields must be corrected for isotopic abundance of ¹⁸⁹O; the elastic scattering yields can be treated as though the elastic scattering cross sections for all Os isotopes were the

same. The comparison of natural Os total cross sections with those measured¹⁰ for ^{189}Os and the small abundances of other isotopes lead to possible isotopic corrections to elastic scattering less than 1%. These corrections were ignored.

The cylindrical Os and Pb samples were mounted at 0° with their axes perpendicular to the scattering plane, the usual symmetric geometry for neutron scattering experiments, and at 4.5 cm from the LiF target. The 90° detector was mounted at 34.3 cm from the sample for the 63.5- and 73.3-keV measurements, and at 37 cm for the 97.5-keV runs. The samples were contained in low-mass steel-wire baskets of about 0.072 g. An empty wire basket of 0.08 g was mounted for background runs; no peaks from the basket were evident above the time-unrelated background. The location of the samples was such that they subtended a half-angle which corresponded to a neutron energy spread of 2 keV, insignificant compared to the overall incident energy spread of 6 keV.

Thirty-four runs of about 1 h duration each were made with the ^{189}Os sample at 73.3 keV incident, interspersed with 17 background runs and 20 Pb sample runs. The repeated, interspersed runs enabled us to monitor for minor instabilities in the TOF electronics and correct for those later when the separate runs were combined into a single spectrum for each sample for yield analysis. A similar number of runs were taken at 63.5 keV incident, and about half that number at 97.5 keV. As for the data taken at 73.3 keV, all runs for each sample were combined into a single spectrum for yield analysis at each incident energy.

III. DATA REDUCTION, EFFICIENCY AND SAMPLE-SIZE CORRECTIONS

A. Peak shapes and yields

Each peak in each of the three combined ^{189}Os spectra, for each of the three incident energies, and each peak in the combined Pb sample spectra, was modeled with a shape which combined two Gaussians convoluted with an exponential, to reproduce the asymmetric shapes and exponential tails always encountered in TOF neutron scattering experiments. The combined data for scattering from the Pb sample at 63.5 keV incident and a fit to the data are shown in Fig. 1. The shape parameters determined from this fit were then inserted into the peak analysis program, SAN12, designed in this laboratory to fit the peaks from scattering. The peak-fitting program was told to find two peaks in the ^{189}Os spectrum, with widths correctly correlated for TOF spectra, and separated by an excitation energy of 36.2 keV.

The width of TOF peaks changes as a function of flight time from the scattering sample to the detector because a fixed energy spread translates into a varying time spread. The widths of our peaks always have components from fixed time spreads in our measurements, such as beam pulse width and time spread intrinsic to the detectors, and a component from the fixed energy spread arising from the thickness of the LiF target. The beam-pulse width was just under 3 ns, and the detector intrinsic time

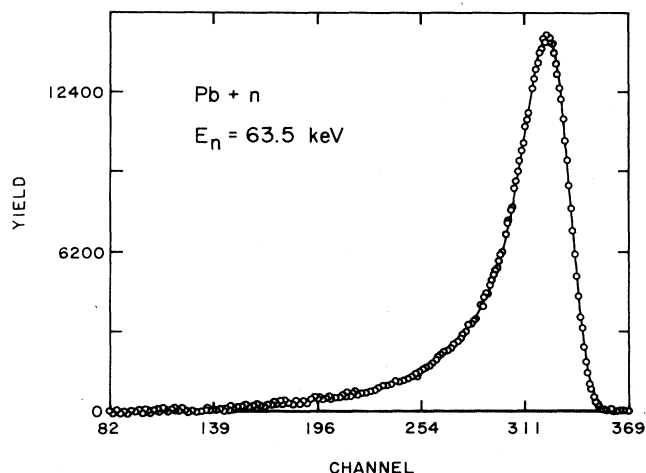


FIG. 1. Scattered neutron spectrum for the natural Pb sample whose size is the same as that for the ^{189}Os sample. The solid curve is the result of a fit to the spectrum.

spread was also about 3 ns. The overall time resolution extracted from the spectra was about 4.0 ns. Besides the 36.2-keV $\frac{1}{2}^-$ level, there is also a $\frac{9}{2}^-$ level at 30.8 keV excitation energy; but calculations show that the cross section to it should be only 7% that for the $\frac{1}{2}^-$ level. We did not attempt measurement of the very small cross section for the $\frac{9}{2}^-$ level.

The result of the fit to the ^{189}Os spectrum is shown in Fig. 2, with an expanded inset to show the region of the inelastic group. The result of the parameter search was an incident energy and peak width for elastic scattering

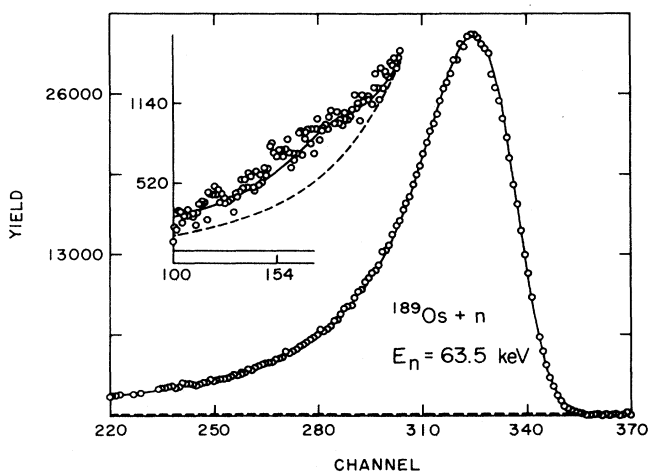


FIG. 2. Scattered neutron spectrum for the ^{189}Os sample. The solid curve is a fit to the spectrum using the shape parameters from the fit to the spectrum of Fig. 1. The inset shows the channel region where the inelastic scattering group appears. The dashed curve of the inset shows the tail of the elastic fit as determined from the fit of Fig. 1. The solid curve is the fit to the combined elastic and inelastic scattering groups, with the separation of the two groups constrained by scattering kinematics.

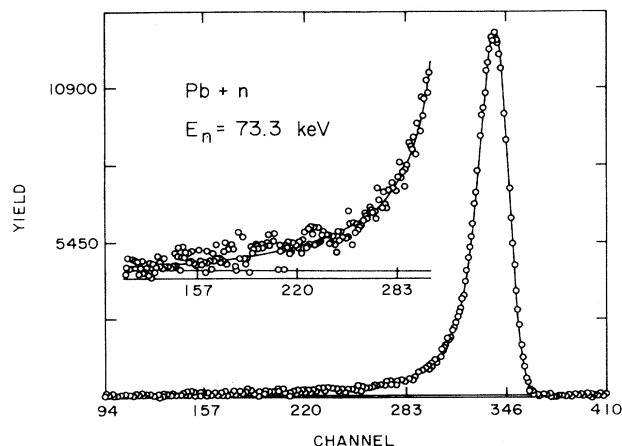


FIG. 3. Scattered neutron spectrum for the natural Pb sample at an incident energy of 73.3 keV. The solid curve is the fit to the spectrum, with the details of the fit in the tail region shown in the inset.

identical to those found from the search procedure for the Pb spectrum of Fig. 1. The dashed curve shown in the inset is the tail which would have been predicted by the Pb fit were there no inelastic group present. The constancy of the incident energy extracted from the fitting process was consistent with the fact that the 0° monitor of incident neutron flux was used to maintain the incident neutron energy constant to within 0.1 keV during the course of all runs at each of the three incident neutron energies.

The same peak-fitting procedure was followed for the scattering data measured at 73.3 keV incident, with the fits shown in Figs. 3 and 4, again with expanded insets to show the quality of the fits for the Pb tail region, and

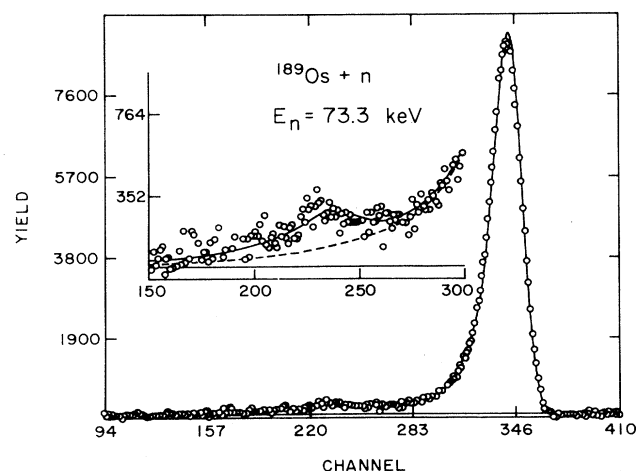


FIG. 4. Scattered neutron spectrum from ^{189}Os . The solid curve is the fit to the combination of elastic and inelastic scattering to the $\frac{1}{2}^-$ level at 36.2-keV excitation energy. The shape parameters are those of the Pb fit of Fig. 3. The dashed curve in the inset shows the elastic tail extended into the region of inelastic scattering.

those including the inelastic scattering group for the Os runs, again with all Os runs combined. Similar but independent peak analyses were made at ORELA for the runs at 73.3- and 97.5-keV incident neutron energy with very similar results. The analysis made at 97.5 keV incident is shown in Fig. 5, again with the Pb peak shape and kinematics constraining the analysis of the Os spectrum.

B. Efficiency corrections and normalization of yields

Peak yields had to be corrected for the energy dependence of the detection efficiency of the majority logic detector, and corrected for the effects of attenuation and multiple scattering. The neutron energy dependence of the detection efficiency was measured with two methods. Thick LiF target spectra were measured with a proton bombarding energy which provided neutron energies from 30 keV at threshold to 103 keV in a single TOF spectrum. The yields as a function of delay time, or equivalently neutron energy, were then unfolded into $^7\text{Li}(p,n)$ relative yields as a function of neutron energy using known proton stopping powers. The recorded yields as a function of neutron energy divided by the well-known $\text{Li}(p,n)$ cross sections²³ then provided relative efficiencies for the majority logic detector which are shown as the circular points and solid curve in Fig. 6.

A second method of determining the efficiency was used to check the thick target results for neutron energies $E_n > 60$ keV. This second method involved measuring neutron yields from a thin LiF target as a function of angle at the same proton energy as that incident for the thick target measurements, and then dividing those yields by the known angle-dependent cross sections of the $^7\text{Li}(p,n)$ reaction²⁴ to obtain the relative efficiencies. This latter method was deemed not reliable for neutron energies well below 60 keV, or detection angles beyond 45° . The crosses shown in Fig. 6 are from this method.

C. Sample-size effects

Sample-size effects arise from neutron attenuation, multiple scattering, and angular spread of the sample at the neutron source combined with the anisotropy of elastic scattering. Inelastic scattering yields are isotropic, as had been determined by direct measurements in the earlier work⁹ on scattering for ^{187}Os . The outgoing neutron energy to the $\frac{1}{2}^-$ level in this experiment is 61 keV, compared to 50 keV in the cited work. Thus the isotropy observed there would be expected here as well. The statistical-model calculations show an expected variation of 1% in differential scattering cross section between 0° and 90° .

Neutron attenuation alters the effective incident neutron flux from that which would be present without a scattering sample. Since we obtain cross sections through normalization of measured yields to measured total cross sections, attenuations do not affect our measurements. Multiple scattering in these cylindrical scattering samples decreases the angular anisotropy of elastic scattering yields. The elastic scattering angular distributions for

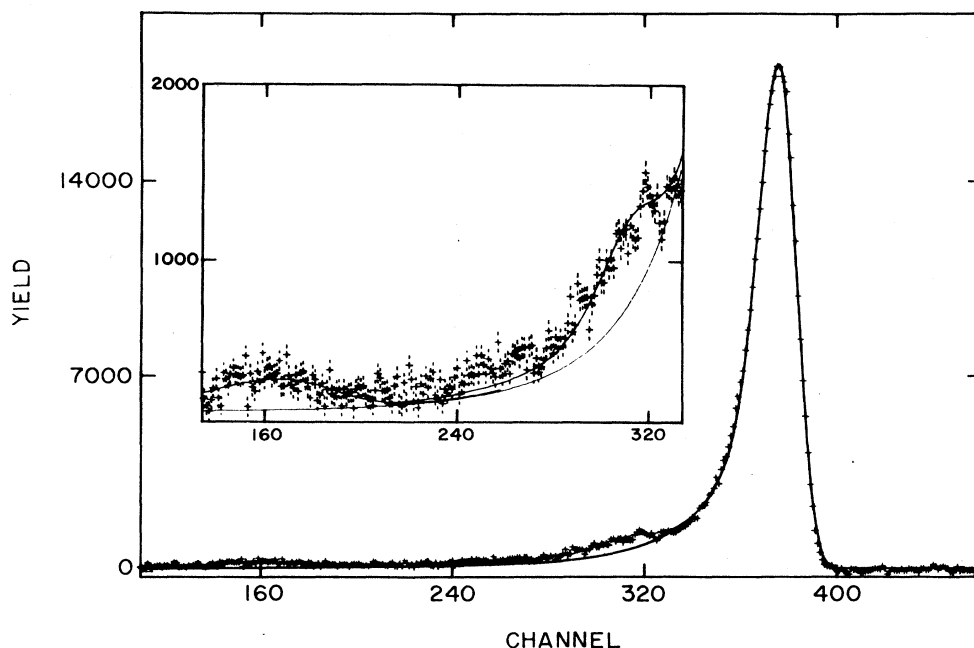


FIG. 5. Scattered neutron spectrum from ^{189}Os at an incident energy of 97.5 keV. The solid curve is a fit using shape parameters obtained from a fit to scattering from the Pb sample. The inset shows the inelastic scattering regions expanded to show the fit to the combined elastic and two inelastic scattering groups for levels at 36.2 and 69.6 keV excitation energy. The lower curve in the inset shows the extension of the elastic tail into the inelastic scattering region.

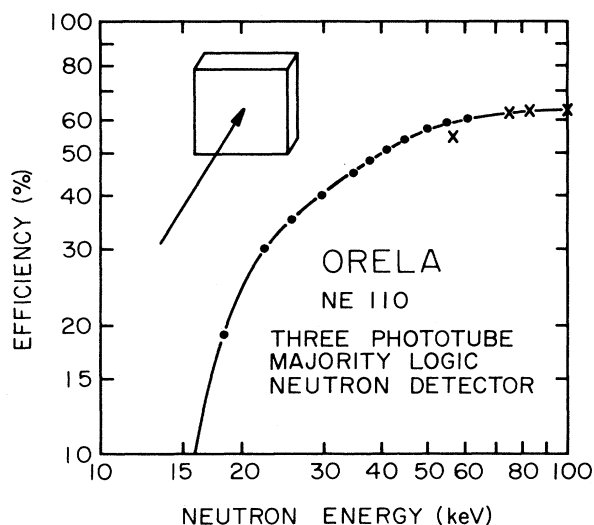


FIG. 6. The relative efficiency, or neutron energy dependence of the efficiency, of the majority logic detector as a function of neutron energy as measured with two techniques. The crosses represent the results of normalizing differential yield measurements of the $^7\text{Li}(p,n)^7\text{Be}$ source reaction as a function of reaction angle to the known differential cross sections of the $^7\text{Li}(p,n)^7\text{Be}$ reaction. The circular points and solid curve are efficiency measurements from thick target neutron spectra, which are unfolded into 0° yields as a function of proton energy in the ^7Li target using procedures described in the text. The thick target efficiencies, represented by the solid curve, were found to be the same as those which had been obtained in Ref. 8 for the same detector.

^{187}Os and ^{188}Os were found⁹ to be asymmetric about 90° , with a simple $\cos\theta$ dependence. Since our detector was located at 90° , anisotropy changes did not affect normalization.

Our procedure relies only upon the ratio of efficiency-corrected scattering yields for inelastic to elastic scattering. This ratio is altered by multiple scattering in which one of the events is an inelastic one. Such corrections are small, because the inelastic to elastic ratio is $\leq 6\%$. Small corrections were necessary at 63.5 keV, where a 1% correction applied, and 97.5 keV incident, where the ratio of inelastic to elastic scattering was increased by 2% through multiple scattering. These multiple scattering corrections to the ratios of inelastic to elastic scattering yields were calculated using analytic approximations developed by Engelbrecht.²⁵

D. Cross-section normalization

The procedure used to turn efficiency corrected yields into differential scattering cross sections relied for normalization upon the accurate total cross sections measured at ORELA (Ref. 10). These total cross sections were measured with the usual white source techniques,²⁶ using two different sample thicknesses. As noted near the beginning of Sec. II, the ^{189}Os sample was in the form of eight thin metal wafers, each of 1.27 cm diameter and about 0.5-mm thick. Total cross sections were measured with two different sample thicknesses, one using only two of the eight wafers, and the other using six of them. The results of the two sets of measurements were consistent with each other, when each set was averaged over an in-

cident energy interval of 8 keV, to within better than 2%.

The elastic and inelastic scattering yields of this experiment were corrected for the energy dependence of detection efficiency and sample-size effects, and then normalized, effectively, to the difference between the measured total and neutron capture cross sections.²⁷ The procedure for normalizing corrected yields to cross sections was developed to accommodate the fact that measurements were not available for the $\frac{9}{2}^-$ excited level. Since we could only estimate the cross section for that level, the normalization procedure used was an iterative one. The correction for the unobserved $\frac{9}{2}^-$ level is small, since its cross section is calculated to be only 3.8% of the nonelastic cross section, which is the relevant comparison for estimating the effect of that level on our normalization procedure.

The first step in our iterative normalization procedure used calculated inelastic scattering cross sections for the $\frac{9}{2}^-$ level. These were combined with the measured (n, γ) and inelastic scattering cross sections to give a first estimate of the nonelastic cross section. The second step of the iteration procedure simply involved summing all measured inelastic scattering cross sections, the calculated value for the $\frac{9}{2}^-$ level, the measured (n, γ) cross sections,²⁷ and the elastic scattering cross sections and correcting the normalization factor to achieve consistency with the total cross section.

IV. RESULTS AND UNCERTAINTIES

The measured total cross sections, to which normalization is made, and the capture cross sections as a function of neutron energy are shown in Fig. 7. Also shown in Fig. 7 are the capture cross sections measured for the $\frac{1}{2}^-$ ground state of ^{187}Os , for completeness of comparisons with the statistical model. The dashed histogram shown with the total cross sections in the upper panel is the result of averaging the fine structure data over energy intervals of about 8 keV. The solid curve shown with the data is the result of model calculations. The points shown in the lower panel are the energy-averaged capture cross section measurements, and the curves are statistical-model calculations to be discussed in the next section.

The measured inelastic scattering cross sections for the 36.2-keV level of ^{189}Os are the points plotted in Fig. 8 near 0.5 b, with theoretical curves. We also show, for ease of comparison, the earlier,^{8,9} larger measurements of inelastic scattering to the first excited level of ^{187}Os . The large difference between results for the two nuclei reflects the spin differences of the two ground and two excited levels, and the different scattering kinematics for the two nuclei.

Our measured inelastic scattering cross sections differed from model calculations by an average of <10%. The uncertainties of these comparisons propagate into our normalization procedure. Uncertainties quoted²⁷ for the (n, γ) cross sections are about $\pm 5\%$. The resultant uncertainty of the normalization procedure is about $\pm 7\%$. The total cross sections to which we are normalizing our yields have an uncertainty of $\pm 2\%$, which we

combine arithmetically with the uncertainty of the normalization procedure. Many tests of the peak-fitting procedures using SAN12 showed that the yield ratios obtained for different but acceptable fits varied no more than $\pm 5\%$, an uncertainty combined in quadrature with that of the energy dependence of neutron detection efficiency.

The relative efficiency uncertainty, as noted above and as is evident in Fig. 6, ranges from $\pm 2\%$ for scattered neutron energies of 60 keV to $\pm 12\%$ for 27-keV neutrons. This is the dominant uncertainty for two of the measured inelastic scattering cross sections. Thus, the uncertainties of our measured values ranges from 11 to 15%. The uncertainties of sample-size corrections are insignificant.

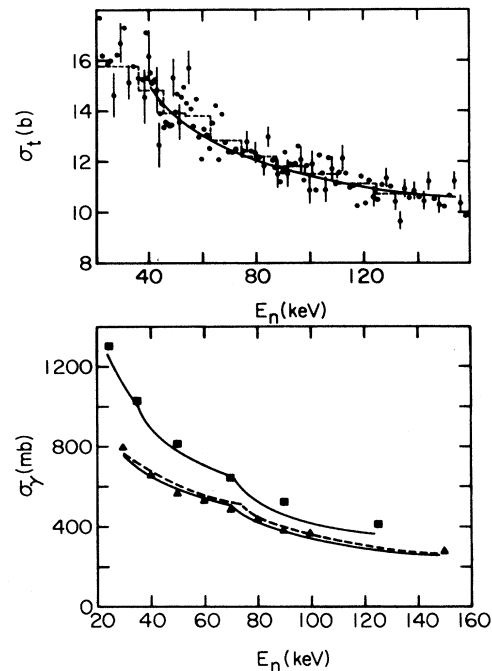


FIG. 7. The top panel shows total cross sections measured at ORELA using TOF techniques. Many more points are measured than are shown, with uncertainties. The dashed histogram is a 50 point average, which amounts to about an 8 keV average near 80 keV neutron energy. The solid curve is the potential-model calculation as described in the text. The bottom panel shows calculated and measured capture cross sections for both ^{187}Os and ^{189}Os . The upper set of (square) points are energy-averaged measurements for ^{189}Os , and the solid curve provides statistical-model calculations using the methods and parameters of Ref. 9 or the dipole parameters of Table I; both give the same result for that nucleus. The lower, triangular points are energy-averaged, measured capture cross sections for ^{187}Os , and the solid curve through those measurements represents the statistical-model calculations with the same potential and dipole parameters as for ^{189}Os following the parametrization of Ref. 9. The dashed curve results from the use of the measured dipole parameters of Table I.

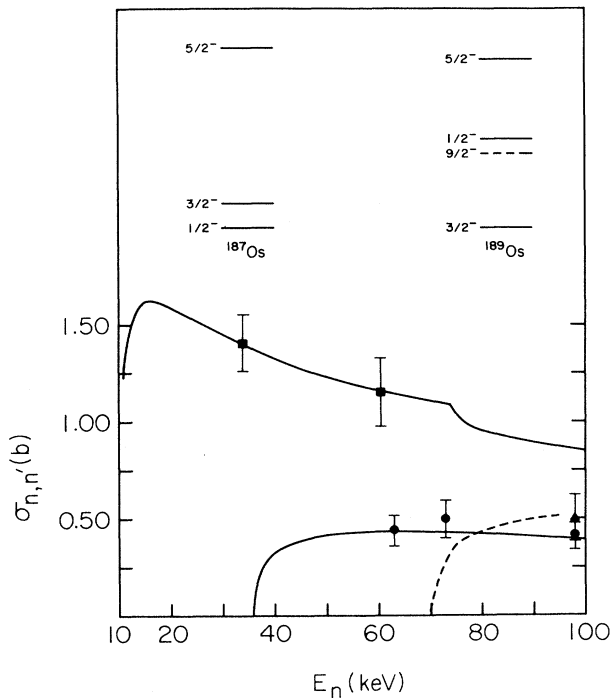


FIG. 8. Measured and calculated inelastic scattering cross sections for both ^{187}Os and ^{189}Os . The square points are measurements for ^{187}Os reported in Refs. 8 and 9. The curve is a statistical-model result as described in the text. The circular and triangle points are measurements for the $\frac{1}{2}^-$ and $\frac{5}{2}^-$ levels of ^{189}Os , respectively. The solid and dashed curves are the associated statistical-model calculations. Note that the abscissa scale has a depressed zero.

V. INTERPRETATION AND SUMMARY

A. Scattering model and comparisons with measurements

The total, capture, and inelastic scattering cross sections of Figs. 7 and 8 are modeled as statistical processes based on a scattering potential, using the form of the statistical model provided by Tepel, Hofmann, and Herman.¹⁶ The scattering potential must be determined with high confidence, and the gamma-ray strength for the capture channels must be well fixed. Considerable information is available to fix the neutron scattering potential. This includes very-low-energy scattering properties, such as the *s*-wave strength functions,^{11,27} and total cross sections as a function of neutron energy. A potential had been carefully developed⁹ to fit these scattering properties for ^{187}Os , as well as the measured asymmetry of elastic neutron scattering for both ^{187}Os and ^{188}Os . The *s*-wave strength function, scattering length, total cross sections, and elastic scattering cross sections for ^{187}Os and elastic scattering cross sections for ^{188}Os were all well described.⁹ This potential, the gamma-ray strength and the statistical model now serve as the basis of all analyses to be reported here. The scattering potential and neutron capture parameters used in this analysis are presented in Table I. It is important to realize that present, successful

TABLE I. Scattering potential and dipole resonance parameters. The symbol V denotes depth of the real central potential. W_D denotes surface absorptive potential, with Woods-Saxon derivative form factor, both these potential parameters are given in MeV. The r_k denote radius parameters and the a_k denote diffusenesses, both in fm. The symbol E denotes incident neutron energy in MeV. The parameters of the $E1$ dipole resonance are Γ_g , the dipole width, σ_0 , the peak dipole cross section, and E_D , the resonance energy. The product $\Gamma_g \sigma_0$ represents the strength of the resonance, maintained the same for both odd- A nuclei.

$V = 47.4 - 0.27E$, $\tau_v = 1.22$, $a_v = 0.63$
$W_D = 9.57 + 0.45E$, $r_D = 1.26$, $a_D = 0.47$
Measured dipole parameters for ^{187}Os :
$\sigma_0 = 230$ mb, $\Gamma_g = 2.76$ MeV, $E_D = 12.81$ MeV
Measured dipole parameters for ^{189}Os :
$\sigma_0 = 250$ mb, $\Gamma_g = 2.60$ MeV, $E_D = 12.68$ MeV

^{189}Os analyses are made without altering a single parameter from those determined⁹ as necessary for ^{187}Os in 1983.

B. Capture cross sections

The modified statistical model for neutron induced reactions and the Brink-Axel hypothesis for γ -ray strength functions argues that the γ -ray transmission coefficients should have the energy dependence of the tail of the giant electric dipole ($E1$) resonance,²⁸ as had been noted in the previous measurements and analyses⁹ for ^{187}Os . A thorough analysis of average neutron capture cross sections based on this assumption had been carried out many years ago by Johnson.²⁸ He developed a systematics for describing the neutron energy dependence of these cross sections using an $E1$ model with "resonance" parameters adjusted to fit the systematics of low-energy neutron capture over a large range of nuclei; the parameters so deduced²⁸ were not actual $E1$ resonance parameters, but were a parametrization of low-energy neutron capture cross sections. Thus, our earlier analyses for ^{187}Os employed a width parameter set to 1.95 MeV, as called for in Johnson's systematics.²⁸ The peak capture cross section on the $E1$ resonance was then adjusted to 490 mb to provide a good description of the capture cross sections.⁹ This procedure used the dipole form to represent energy dependence, but fixes the strength to accommodate direct capture as well as dipole tail capture.²⁸ (The peak cross section used in Ref. 9 was incorrectly quoted in Table 5 of Ref. 27.)

The actual $E1$ resonance parameters for ^{188}Os and ^{190}Os have been measured in (γ, xn) cross-section studies.²⁹ Thus, we made statistical-model calculations of the (n, γ) cross sections of Fig. 8 using parameters drawn from Johnson's systematics²⁸ and also using the measured $E1$ parameters. For both sets of calculations the γ -ray strength was normalized to reproduce the $^{189}\text{Os}(n, \gamma)$ cross sections in Fig. 8. The solid curve represents both sets of calculations for that nucleus. The dashed curve shown for ^{187}Os results from using the actual²⁹ resonance parameters, and again keeping the γ -ray strength the same for both nuclei; the solid curve results from the

methods of Ref. 9.

The striking similarity of the level structures of the two nuclei justifies treating both of them on a common basis, including the common γ -ray strength. Also the average of measured radiation widths for low-energy neutron capture resonances has been shown to be the same in the two nuclei.²⁷ A similar conclusion can be drawn from the (γ, n) and $(\gamma, 2n)$ experiments of Berman *et al.*²⁹ Their studies include neutron emission cross sections over the $E1$ resonance region for both ^{188}Os and ^{190}Os ; the photon induced strength is quite comparable for the two nuclei, even including the degree of quadrupole splitting of the $E1$ resonance. It is well known^{29,30} that the degree of dipole splitting is a measure of the low-lying $E2$ strength of nuclei. This experiment, as well as the Coulomb excitation experiment,²⁰ show that the structures and photon strengths of the two nuclei are very similar.

The really important results of these model tests are the ratios of capture cross sections for the two nuclei; the ratios are the tests of predicting capture on both the $\frac{1}{2}^-$ ground state and $\frac{3}{2}^-$ excited level of ^{187}Os . The fact that very similar calculated capture cross sections result from using rather different parametrizations of the γ -ray strength shows that the neutron energy dependence and ratios of capture cross sections are not sensitive to details of the parametrization of the γ -ray strength.

C. Summary of results

All parameters of the models having been set,⁹ tests are shown in Figs. 7 and 8. The upper panel of Fig. 7 shows the total cross-section data taken at the Oak Ridge Electron Linear Accelerator (ORELA) for ^{189}Os . The solid points are the measured total cross sections; the solid curve shows the accuracy of the potential description. The lower curves of the bottom panel of Fig. 7 show data and calculations for neutron capture by the $\frac{1}{2}^-$ ground state of ^{187}Os . The triangle shaped points are the

energy-averaged data, and the curves through the points are the statistical-model calculations using the two different approaches to fixing the γ -ray strength, one using the method used in Ref. 9 and the other using actual $E1$ resonance parameters. The cross sections in the top panel and the lower curves of the lower panel represent real predictions, since no parameters were adjusted to provide those fits. The square points are the energy-averaged capture cross sections²⁷ for the $\frac{3}{2}^-$ ground state of ^{189}Os , and the curve through the points represents the model calculations. The agreement is excellent below 70 keV, and still within about 10% above that energy.

The capture cross sections of Fig. 7 are well described with a statistical model which includes J -dependent γ -ray transmission coefficients. Were J -independent capture strengths to have been used, the ratio of cross sections would be altered at least 25%, outside the uncertainties of the measurements for the two nuclei. This is an important point with respect to the model to be used for nucleosynthesis of heavy elements by neutron capture. An earlier study of neutron capture resonances for ^{187}Os and ^{189}Os had also led to the conclusion³¹ that the resonance strengths in the two nuclei were clearly those associated with the statistical model.

The model has its most definitive test in Fig. 8, where measurements and calculations of inelastic scattering are presented. The upper curve and two measured points^{8,9} are for ^{187}Os , the nucleus for which the model had been developed. However, it is important to note that no parameters of the model are adjusted to fit these measurements. The potential is developed to represent total and elastic scattering cross sections. These inelastic scattering cross sections are than a prediction.

The lower curves and measured points are for scattering to the $\frac{1}{2}^-$ and $\frac{5}{2}^-$ excited levels of ^{189}Os , the calculations represented by the solid and dashed curves, respectively. The lowest few levels of each of the two nuclei are

TABLE II. Low-energy scattering properties and comparisons of measured (m) and calculated (c) cross sections. The parameter s_0 is the s -wave strength function; s_1 is the p -wave strength function; R' is the scattering length. The E_n are incident neutron energies, and σ_t are total cross sections; $\sigma_{n,\gamma}$ are capture cross sections, and $\sigma_{n,n'}$ are inelastic scattering cross sections to the $\frac{1}{2}^-$ excited level. The $\Delta\sigma$ are uncertainties in the measured inelastic scattering cross sections.

Nucleus:	Low-energy scattering properties					
	^{187}Os		^{189}Os			
	Calculated	Measured	Calculated	Measured		
$s_0(\times 10^4)$	3.5	3.2	2.8	2.9		
$s_1(\times 10^4)$	0.98		0.9			
R'	8.6 fm		8.7 fm			
Comparisons of cross sections for ^{189}Os						
E_n (keV)	σ_t^c (b)	σ_t^m (b)	$\sigma_{m\gamma}^c$ (mb)	$\sigma_{m\gamma}^m$ (mb)	$\sigma_{nn'}^m$ (mb)	$\Delta\sigma$ (mb)
63.5	12.84	13.2	683	695	427	50
70			649	641		
73.3	12.28	12.2	587		480	30
97.5	11.2	11.7	427	495	386	30

sketched in the top part of the figure, where one sees the good correspondence between the two structures up to an excitation energy of about 100 keV. The $\frac{9}{2}^-$ level is also found in ^{187}Os , just above the highest incident energy reached in this experiment.

The low-energy scattering properties and total and partial cross sections obtained in this study are presented in Table II. The very good agreement shown in Table II is striking confirmation of a model developed three years before these measurements, although the parameters of the model are published here for the first time.

D. Impact on the Re/Os nucleochronology and Os nucleosynthesis

The importance of excited-state capture in a stellar environment had first been cited by Woosley and Fowler⁷ in their review of the Re/Os nucleochronology. They introduced the influence of excited-state capture in terms of the ratio of two Maxwellian-averaged capture cross-section ratios. Each capture cross-section ratio is of Maxwellian-averaged capture in ^{186}Os to that in ^{187}Os . One ratio, averaged in the stellar environment, is divided by that averaged in a laboratory, where no excited state is involved. This factor, called F by Woosley and Fowler, and more recently²⁷ named F_{67} , was shown⁹ to be $F_{67}=0.8$, a value restated recently when the ^{189}Os capture cross-section measurements were reported.²⁷ The

ratio F_{67} should be rather temperature independent, for stellar interior temperatures deemed to be realistic, even though the Maxwellian capture cross sections themselves are temperature dependent. The insensitivity of F_{67} to temperature reflects the common energy dependence of all of the capture cross sections. Thus, the role of neutron capture in the s -process abundance of ^{187}Os should be well defined, with the value $F_{67}=0.80\pm 0.01$, as determined in several previous studies,^{9,27} well confirmed in this study. It is gratifying to see that the modified form of the statistical model, which has been shown to be so effective for neutron scattering in complex nuclei at incident neutron energies from 1 to 3 MeV, works very well also for incident energies below 100 keV.

ACKNOWLEDGMENTS

The authors acknowledge with great appreciation several conversations and exchanges of correspondence with Prof. Emeritus W. A. Fowler of Cal Tech, whose advice on the uncertainties of the different nucleochronologies was invaluable. This project was supported in part by The National Science Foundation through grants PHY-8403278 and PHY-8702369. This work was also supported by the U.S. Department of Energy under contracts DE-FG02-87ER40326 with Denison University and DE-AC05-84OR21400 with Martin Marietta Energy Systems, Inc.

*Permanent address: Department of Physics, Denison University, Granville, OH 43023.

†Permanent address: Nichols Research Corporation, Huntsville, AL 35802.

‡Permanent address: Institute of Atomic Energy, Beijing, People's Republic of China.

§Permanent address: Engineering Physics Division, ORELA, Oak Ridge National Laboratory, P.O. Box 2008, Oak Ridge, TN 37831-6354.

¹D. D. Clayton, *Astrophys. J.* **139**, 637 (1964).

²Jean-Marc Luck and Claude J. Allegre, *Nature (London)* **302**, 130 (1983).

³M. Lindner, D. A. Leich, R. J. Borg, G. P. Russ, J. M. Bazan, D. S. Simons, A. R. Date, University of California Radiation Laboratory Report UCRL-92893, 1985; R. J. Walker and J. W. Morgan, *Science* **243**, 519 (1989).

⁴K. Yokoi, K. Takahashi, and M. Arnould, *Astron. and Astrophys.* **117**, 65 (1983).

⁵J. Browne and B. L. Berman, *Nature (London)* **263**, 197 (1976); J. C. Browne and B. L. Berman, *Phys. Rev. C* **23**, 1434 (1981).

⁶R. R. Winters, R. L. Macklin, and J. Halperin, *Phys. Rev. C* **21**, 563 (1980).

⁷S. E. Woosley and William A. Fowler, *Astrophys. J.* **233**, 411 (1979).

⁸R. L. Macklin, R. R. Winters, N. W. Hill, and J. A. Harvey, *Astrophys. J.* **274**, 408 (1983).

⁹R. L. Hershberger, R. L. Macklin, M. Balakrishnan, N. W. Hill, and M. T. McEllistrem, *Phys. Rev. C* **28**, 2249 (1983).

¹⁰R. R. Winters, R. F. Carlton, N. W. Hill, and J. A. Harvey, *Proceedings of the Conference on the 50th Anniversary of the Neutron and its Applications*, Cambridge, England (unpublished); R. R. Winters, R. F. Carlton, J. A. Harvey, and N. W.

Hill, *Phys. Rev. C* **34**, 840 (1986).

¹¹R. R. Winters, R. F. Carlton, J. A. Harvey, and N. W. Hill, *Proceedings of the International Conference on Nuclear Data for Science and Technology*, Antwerp, 1982 (unpublished).

¹²J. W. Tepel, H. M. Hofmann, and H. A. Weidenmuller, *Phys. Lett.* **49B**, 1 (1974).

¹³R. L. Harper, J. D. Brandenberger, and J. L. Weil (unpublished).

¹⁴M. C. Mirzaa, J. P. Delaroche, J. L. Weil, J. Hanly, and M. T. McEllistrem, *Phys. Rev. C* **32**, 1488 (1985).

¹⁵S. E. Hicks, Z. Cao, J. L. Weil, J. M. Hanly, and M. T. McEllistrem (unpublished).

¹⁶J. W. Tepel, H. M. Hofmann, and M. Herman, in *Proceedings of the International Conference on Nuclear Cross Sections for Technology* [National Bureau of Standards Special Publication 594, 1979, edited by J. L. Fowler, C. H. Johnson, and C. D. Brown, p. 762].

¹⁷J. M. Hanly, Ph.D. dissertation, University of Kentucky, 1987.

¹⁸P. A. Moldauer, in *Proceedings of the International Conference on Interactions of Neutrons with Nuclei*, U.S. Energy Research and Development Administration Report CONF-760715, 1976, edited by E. Sheldon, p. 243; P. A. Moldauer, *Bull. Am. Phys. Soc.* **28**, 688 (1983).

¹⁹R. R. Winters and R. L. Macklin, *Phys. Rev. C* **25**, 208 (1982).

²⁰S. Jha, W. A. Seale, R. V. Ribas, E. W. Cybulska, and M. N. Rao, *Phys. Rev. C* **28**, 921 (1983).

²¹A. O. Hansen and J. L. McKibben, *Phys. Rev.* **72**, 673 (1947).

²²N. W. Hill, J. A. Harvey, D. J. Horen, G. L. Morgan, and R. R. Winters, *IEEE Trans. Nucl. Sci.* **NS32**, 367 (1985).

²³J. H. Gibbons and R. L. Macklin, *Phys. Rev.* **114**, 571 (1959); H. J. Kim, W. T. Milner, and F. K. McGowan, *Nucl. Data*

- Tables 1, 225 (1966).
- ²⁴Horst Liskien and Arno Paulsen, *At. Data Nucl. Data Tables* **15**, 57 (1975).
- ²⁵C. A. Engelbrecht, *Nucl. Instrum. Methods* **93**, 105 (1971).
- ²⁶J. A. Harvey and N. W. Hill, *Nucl. Instrum. Methods* **162**, 507 (1976); D. C. Larson, N. M. Larson, J. A. Harvey, N. W. Hill, and C. H. Johnson, Oak Ridge National Laboratory Report ORNL/TM-8203, 1983.
- ²⁷R. R. Winters, R. L. Macklin, and R. L. Hershberger, *Astron. Astrophys.* **171**, 9 (1986).
- ²⁸C. H. Johnson, *Phys. Rev. C* **16**, 2238 (1977).
- ²⁹B. L. Berman, D. D. Faul, R. A. Alvarez, P. Meyer, and D. Olson, *Phys. Rev. C* **19**, 1205 (1979); Samuel S. Dietrich and Barry L. Berman, *At. Data Nucl. Data Tables* **38**, 199 (1988).
- ³⁰M. T. McEllistrem, in *Proceedings of the Fourth Conference, Scientific & Industrial Applications of Small Accelerators*, edited by J. L. Duggan and I. L. Morgan (Institute of Electrical and Electronic Engineers, New York, 1976), p. 373; P. Carlos, H. Beil, R. Bergere, A. LePrete, A. de Miniac, and A. Veysi-ere, *Nucl. Phys.* **A225**, 171 (1974).
- ³¹A. Stolovy, A. I. Namenson, and B. L. Berman, *Phys. Rev. C* **14**, 965 (1976).